Available online at www.sciencedirect.com
SCIENCE DIRECT®
Combustion and Flame 143 (2005) 450–470
Combustion and Flame
www.elsevier.com/locate/combustflame

The influence of chemical mechanisms on PDF calculations of nonpremixed piloted jet flames ☆

Renfeng Richard Cao *, Stephen B. Pope

Mechanical and Aerospace Engineering, Cornell University, 245 Upson Hall, Ithaca, NY 14853, USA

Received 9 April 2005; received in revised form 28 August 2005; accepted 31 August 2005

Available online 10 October 2005

Abstract

Seven different chemical mechanisms for methane are used in PDF model calculations of the Barlow and Frank flames D, E, and F in order to investigate the ability of these mechanisms to represent the local extinction, reignition, and other chemical phenomena observed in these nonpremixed piloted jet flames. The mechanisms studied range from a 5-step reduced mechanism to the GRI3.0 mechanism which involves 53 species. As in several other recent studies, we use the PDF method based on the joint probability density function of velocity, turbulence frequency, and composition. Extensive tests are performed to ensure the numerical accuracy of the calculations, to relate them to previous calculations based on the same model, and to reexamine the sensitivity of the calculations (especially of flame F) to uncertainties in the pilot temperature and the treatment of radiation. As has been observed in other studies of laminar and turbulent nonpremixed flames, we find that the GRI3.0 mechanism overpredicts the levels of NO, typically by a factor of 2. Apart from this, the GRI3.0 and GRI2.11 mechanisms yield comparably good agreement with the experimental data for all three flames, including the level of local extinction and the conditional means of major and other minor species. Two augmented reduce mechanism (ARM1 and ARM2) based on GRI2.11 and containing 16 and 19 species are slightly less accurate; while the 5-step reduced mechanism and two C_1 skeletal mechanisms containing 16 species display significant inaccuracies. An examination of the autoignition and laminar-flame behavior of the different mechanisms confirms (with some exceptions) expected trends: there is an association between long ignition delay times, small extinction strain rates, and high levels of local extinction. This study again demonstrates the ability of the joint PDF method to represent accurately the strong turbulence–chemistry interactions in these flames, and it clarifies the necessary level of description of the chemical kinetics.
© 2005 The Combustion Institute. Published by Elsevier Inc. All rights reserved.

Keywords: PDF methods; Turbulent flames; Detailed chemistry; Mixing models

1. Introduction

In this work we use PDF methods to study the performance of seven different chemical mechanisms in the calculation of turbulence–chemistry interactions in nonpremixed turbulent flames. The calculations are compared to the experimental data of Barlow

☆ This paper is accompanied by Supplementary material which is available at doi: 10.1016/j.combustflame.2005.08.018.

* Corresponding author. Fax: +1 (607) 255 1222.
E-mail address: rc239@cornell.edu (R.R. Cao).

0010-2180/$ – see front matter © 2005 The Combustion Institute. Published by Elsevier Inc. All rights reserved.
doi:10.1016/j.combustflame.2005.08.018

and Frank [1] which were obtained using the Sydney burner. This burner consists of a central fuel jet and a substantial annular pilot, and it is surrounded by a coflowing air stream. It is most fitting to describe these results in this special issue of Combustion and Flame honoring Bob Bilger. The Sydney burner was developed 20 years ago by Stärner and Bilger [2], with the aim of creating strong turbulence–chemistry interactions in a stable flame with relatively simple fluid mechanics and turbulence structure [3]. The demonstration of local extinction and reignition in these flames earned Masri and Bilger [4] the silver medal of the Combustion Institute in 1988. Single-point laser diagnostics were then applied to these flames (as reviewed by Masri et al. [5]), culminating in the experiments of Barlow and Frank [1] which are the focus of the current work. The subsequent line-imaging measurements of Karpetis and Barlow [6] yielded, in 2004, a second silver medal for work based on the Sydney burner.

The flow parameters and the pilot temperature for the nonpremixed piloted jet methane–air flames D, E, and F are listed in Table 1. The fuel, consisting of 25% methane and 75% air, with a temperature of 294 K, forms the inner fuel jet with a diameter of $D = 7.2$ mm. The flame is stabilized using a pilot with a diameter of $D_\mathrm{p} = 18.2$ mm. The pilot is a burnt lean mixture of C_2H_2, H_2, air, CO_2, and N_2, chosen to have the same elemental composition as methane/air at 0.77 equivalence ratio. The coflowing air stream has a temperature of 291 K. Flame D has a small degree of local extinction, while flames E and F have significant and increasing amount of local extinction, with flame F being quite close to global extinction. (The jet velocity in flame F is over 90% of the estimated blowoff velocity [7].)

In 2000, fifteen years after the development of the Sydney burner, the first modeling studies appeared [8–10] which convincingly and quantitatively described local extinction and reignition in these nonpremixed piloted jet methane flames. These two sets of calculations from Imperial College [10] and from Cornell [8,9] also raised questions about the two modeling ingredients at the core of turbulence–chemistry interactions, namely, the chemical mechanisms and the turbulent mixing model. The two sets of calculations use different mechanisms and different mixing models. The EMST mixing model [11] with model constant $C_\phi = 1.5$ is used in [8,9], whereas the modified Curl model [12,13] with $C_\phi = 2.3$ is used in [10].

Some recent investigations [14–16] have shed light on the relative performance of different mixing models, although our understanding remains incomplete. In general, the calculated amount of local extinction decreases with increasing C_ϕ, and EMST yields less local extinction than modified Curl (for the same value of C_ϕ). The present study aims at advancing our understanding of the issues related to chemical mechanisms.

There are some recent studies of the Barlow and Frank flame D using PDF methods with detailed chemistry [17,18]. Raman et al. [17] calculated the mean profiles and conditional means in flame D using the joint velocity–composition PDF method with the detailed GRI mechanisms (GRI3.0 and GRI2.11) and a 16-species reduced mechanism. In this work, we present PDF calculations of flames D, E, and F using seven different mechanisms. These range from a 5-step reduced mechanism [19,20], to the GRI3.0 detailed mechanism [21] which involves 53 species and 325 reactions. The principal results considered (which are compared to the experimental data [22,23]) are the burning index [8] and means of temperature and species mass fractions conditional on mixture fraction.

In previous work [8,10], it has been found that the calculated level of local extinction (particularly in flame F) is sensitive to the value of the mixing model constant C_ϕ. The base case considered here uses $C_\phi = 1.5$, the value used in conjunction with the EMST [11] model in the previous studies of these flames [8,9]. The present calculations, using the most comprehensive detailed methane mechanisms (i.e., GRI2.11 and GRI3.0), verify that this value of C_ϕ is appropriate. We also investigate the sensitivity of PDF calculations using different chemical mechanisms to the mixing model constant C_ϕ.

Previous calculations [9] have revealed that some flames exhibit a strong sensitivity to the temperature

Table 1
Flow parameters of flames D, E, and F

Flame	Re_jet	$U_\mathrm{j,b}$ (m/s)	$U_\mathrm{p,b}$ (m/s)	U_c (m/s)	T_p (K)	Local extinction
D	∼22,400	49.6	11.4	0.9	1880	Little
E	∼33,600	74.4	17.1	0.9	1880	Moderate
F	∼44,800	99.2	22.8	0.9	1860	Severe

$U_\mathrm{j,b}$ is the bulk velocity for the fuel jet; $U_\mathrm{p,b}$ is the bulk velocity for the pilot; U_c is the coflow velocity; T_p is the pilot temperature.

of the pilot (which is an imposed boundary condition) and to the treatment of radiation. Here we investigate these sensitivities more comprehensively by performing calculations of all three flames with the inclusion and neglect of radiation, and with different values of the pilot temperature.

The behavior of the chemical mechanisms in the joint PDF calculations are related to their behavior in very simple test cases, i.e., autoignition and laminar opposed-flow nonpremixed flame calculations (performed using the code OPPDIF [24]).

In the next section, the submodels used in the joint PDF calculations are briefly introduced. Then the solution domain and boundary conditions are given in Section 3 where the results of tests are reported to establish and quantify the numerical accuracy of the calculations. The numerical method is outlined and the numerical parameters used in these calculations are given in Section 4. The current calculations are compared to previous calculations in Section 5 and the "base case" is defined and investigated. Detailed comparisons of all seven mechanisms are presented in Section 6 based on the results obtained from the PDF calculations, autoignition tests, and the OPPDIF calculations. Results on the effect to radiation, sensitivity to the change of pilot temperature, sensitivity to the change of reaction rates, and the effect of the mixing model constant are also presented in Section 6. The final section provides a summary of the work, and conclusions are drawn.

This paper is accompanied by a file of Supplementary material which contains many more results than can be included in this paper. Specifically, burning indices and profiles of conditional and unconditional means and rms's are shown for 50 joint PDF calculations, corresponding to the base configuration for each flame and each mechanism as well as to perturbations to the pilot temperature and to the treatment of radiation. The Supplementary material is available at doi: 10.1016/j.combustflame.2005.08.018.

2. Joint PDF method and chemical mechanisms

There are several different kinds of PDF methods [25] depending on the set of variables whose joint PDF is considered. The simplest is the composition PDF method [26–28], in which the modeled equation for the joint PDF of composition is solved: the mean flow and turbulence fields are obtained from a separate model calculation. A second PDF method is based on the joint PDF of velocity and composition [17]: in this case a separate model is required for the time or length scale of the turbulence. Attentively, a complete PDF method is based on the joint PDF of velocity, turbulence frequency, and composition [31–35]. This is the method used in the current work, and is hereafter referred to as the joint PDF method.

Table 2
Model constants in the joint PDF models

Constant	Value	Used in
C_0	2.1	SLM
C_Ω	0.6893	Definition of the mean frequency Ω
$C_{\omega 1}$	0.65	Turbulence frequency model
$C_{\omega 2}$	0.9	Turbulence frequency model
C_3	1.0	Turbulence frequency model
C_4	0.25	Turbulence frequency model
C_ϕ	1.5[a]	EMST mixing model

[a] Note that the effect of C_ϕ is studied in Section 6.3.4 by using a range of values, i.e., 1.2, 1.4, 1.5, 2.0, and 3.0.

From the Lagrangian viewpoint, the joint PDF method requires models for velocity, turbulence frequency, and composition following a fluid particle [25,36]. The simplified Langevin model (SLM) is used for the evolution of the particle velocity. The stochastic frequency model of Van Slooten et al. [30] is used for the turbulence frequency of particles, which provides the time scale of turbulence. These models are the same as those used in many previous studies using the joint PDF method, e.g., [8,9,31–35], and are fully described in [36]. The values of the model constants are shown in Table 2, and are the same as those used in [31–34]. The only difference in the constants used in earlier calculations of these flames [8,9] is that there $C_{\omega 1}$ is set to 0.56. A detailed comparison of the current calculations and previous calculations is presented in Section 5, where this difference is discussed.

In PDF methods, the effect of molecular diffusion on the composition is represented by a mixing model. In the present work, the EMST [11] mixing model is used with the mixing model constant C_ϕ set to 1.5 (for the base case) following the works of Xu and Pope [8], and Tang et al. [9]. The impact on the calculations of flame F of changing the value of C_ϕ is examined in Section 6.3.4.

The seven chemical mechanisms considered in this paper are listed in Table 3. The GRI detailed kinetic mechanisms [21] provide the most comprehensive and standardized set of mechanisms for methane combustion. The detailed versions of 2.11 and 3.0 are investigated and denoted as GRI2.11 and GRI3.0, respectively.

The 12-step augmented reduced mechanism [20] without NO obtained from GRI2.11 is denoted as ARM1. This mechanism has been successfully used in the joint PDF calculations of flames D, E, and F performed by Xu and Pope [8]. The corresponding 15-step reduced mechanism which includes NO is denoted as ARM2, and has been successfully used in

Table 3
Chemical mechanisms used in the joint PDF calculations

Mechanism	No. of species	No. of steps	NO species	Reference
GRI3.0	53	325	With NO	[21]
GRI2.11	49	277	With NO	[21]
ARM1	16	12	Without NO	[20]
ARM2	19	15	With NO	[20]
S5G211	9	5	With NO	[19,20]
Skeletal	16	41	Without NO	[37]
Smooke	16	46	Without NO	[38,39]

Table 4
Revised rates in [39] the current Smooke mechanism ($k = AT^b \exp(-E/RT)$)

Reactions	A (K^{-b} mol/(cm^3 s))	b	E (cal/mol)
$CH_4 + H = CH_3 + H_2$	2.2×10^4	3.0	8750.0
$H + O_2 = OH + O$	2.0×10^{14}	0.0	16800.0
$H + O_2 + M = HO_2 + M$	2.1×10^{18} Enhanced third body coefficients H_2O/21.0/ CO_2/5.0/ H_2/3.3/ CO/2.0/ O_2/0.0/ N_2/0.0/	−1.0	0.0

the joint PDF calculations of flames D, E, and F performed by Tang et al. [9]. The 5-step reduced mechanism [19,20] obtained from the GRI2.11 mechanism is denoted as S5G211. A detailed description of the skeletal mechanism is provided by James et al. [37]. The Smooke mechanism is described in [38], but three reactions have been updated [39] and are shown in Table 4. Both the skeletal and Smooke mechanisms do not include any species with more than one carbon atom.

An optically thin limit radiation model is used for the calculations of radiative heat loss [40]. Four gas-phase emitting species H_2O, CO_2, CO, and CH_4 are included in this model, and their Planck mean absorption coefficients are calculated by RADCAL [41]. This is the same radiation model as used in [9]. Because absorption is neglected in the optically thin limit, the present radiation model somewhat overestimates the radiative heat loss from the flames [22,42,43]. On the other hand, adiabatic calculations (with the complete neglect of radiation) obviously underestimate the radiative heat loss. In Section 6.1 we examine the impact on the calculations of the treatment of radiation.

3. Solution domain and boundary conditions

The flames considered in this paper are the series of nonpremixed piloted methane/air jet flames investigated by Barlow and Frank [1], termed Sandia flames D, E, and F. The flow conditions of these three flames are listed in Table 1. These flames are statistically steady 2D axisymmetric, and nonswirling. A polar-cylindrical (z, r) coordinate system is used with the origin at the center of the fuel jet at its exit plane. The computational solution domain is rectangular, of extent $(0, 80D)$ in the axial (z) direction, and $(0, 20D)$ in the radial (r) direction, where D is the diameter of the jet ($D = 7.2$ mm).

At the inlet plane ($z = 0$), the joint PDF of velocity is taken to be joint normal, with the mean velocities and Reynolds stresses obtained from recently updated measured inlet profiles [22,44], which are different from those used in previous calculations [8–10]. (These differences, however, are found to be inconsequential.) The Reynolds normal stress $\langle w^2 \rangle$ in the circumferential direction, which was not measured, is taken to be equal to the radial normal stress $\langle v^2 \rangle$. The turbulence frequency is specified by a gamma distribution and is independent of the velocity. The ratio of production to dissipation of turbulent kinetic energy is specified as unity which, together with the other specified profiles, determines the inlet profile of mean turbulence frequency. The temperature, composition, and density are specified as being uniform in each stream in accord with the experimentally determined values [22]. The coflow boundary ($r = 20D$) is treated as a perfect-slip wall. Symmetry conditions are applied on the centerline ($r = 0$). At the exit plane, in the finite-volume solution of the mean conservation equations, the mean density and the mean axial and radial velocities are extrapolated from the interior, and the pressure is specified to be uniform.

4. Numerical method and accuracy

There are several implementations of particle-mesh methods to solve the modeled joint PDF equations. The computations presented here use a code named HYB2D [31–34] which implements a hybrid finite-volume/particle algorithm. In the hybrid algorithm, the PDF/particle method (particle part) is coupled with a finite volume solver (FV part). The FV part solves the mean conservation equations for mass, momentum, energy and the mean equation of state, and the particle part solves the modeled transport equation for the fluctuating velocity–turbulence frequency–composition PDF. The FV part provides mean fields of velocity, density, and pressure to the particle part and obtains the turbulent fluxes and reaction source terms from the particle part.

The in situ adaptive tabulation (ISAT) algorithm [45] is used to implement the chemistry given by the different mechanisms. A parallel algorithm for the particle part of HYB2D, named domain partitioning of particles [31], is implemented using MPI. These two methods greatly facilitate the calculations presented in this paper.

Systematic tests have been performed on the numerical parameters which affect the accuracy of the calculations to determine appropriate values for use in the current calculations. The procedures to test the effect of these parameters are the same as those described in previous publications [31,35] based on calculations using HYB2D. The only exception is that a different method is used to test the effect of the ISAT error tolerance ε_{tol}, which is specified to control the error incurred in retrieving from the ISAT table.

It has been shown by Liu and Pope [46] that the global error due to ISAT varies linearly with the specified error tolerance ε_{tol}. Following the procedure developed by Liu and Pope [46], calculations of flames E and F were performed (using the skeletal mechanism) for a range of values of ε_{tol}. Fig. 1 shows, plotted against ε_{tol}, the conditional mean temperature and the conditional mean mass fraction of OH, conditional on the mixture fraction ξ being close to stoichiometric (specifically $0.34 \leqslant \xi \leqslant 0.36$). Such conditional means are found to be particularly sensitive to ISAT errors [46], much more so than unconditional means. As may be seen from Fig. 1, for the calculations of flame E, the value of ε_{tol} of 2×10^{-5} results in a global error of substantially less than 2%. However, for the calculations of flame F, the same error tolerance (i.e., $\varepsilon_{\text{tol}} = 2 \times 10^{-5}$) results in a global error of about 5% in the conditional mean temperature and 18% in the conditional mass fraction of OH.

Flame F is quite close to global extinction, which can be brought about by increasing the jet velocity, decreasing the pilot temperature or (in the calculations) by decreasing the value of C_ϕ, as is studied in Section 6.3.4. As global extinction is approached, the calculated flame exhibits increasing sensitivity to these physical and numerical parameters, and indeed at the point of extinction the sensitivities are infinite. As a consequence it is difficult to ensure the numerical accuracy of calculations of flame F when the solution is close to global extinction.

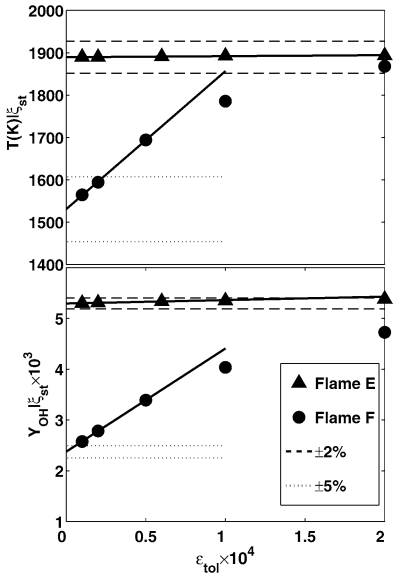

Fig. 1. Effect of the ISAT error tolerance on calculated conditional means using the skeletal mechanism and the EMST mixing model with $C_\phi = 1.5$ for flames E and F at $z/D = 15$. Solid symbols represent calculations for different flames: triangles, flame E; circles, flame F. Solid lines are linear fits through the left three points. Dashed lines are ±2% error and dotted lines are ±5% error relative to the extrapolated ($\varepsilon_{\text{tol}} = 0$) values.

To confirm this interpretation, the calculations of flame F were repeated with the value C_ϕ increased from 1.5 to 2.0, which moves the calculated flame further from global extinction (see Section 6.3.4). This change reduces the error in the conditional mean mass fraction of minor species from 18 to 5% (for the same value of the ISAT error tolerance, $\varepsilon_{\text{tol}} = 2 \times 10^{-5}$).

In the subsequent calculations the ISAT error tolerance is set to $\varepsilon_{\text{tol}} = 2 \times 10^{-5}$. The above results show that the resulting errors are quite small (less than 2%) for calculations far from global extinction (flames D and E); but, unavoidably, these errors become larger for flame F as global extinction is approached.

The numerical parameters used in the current calculations are as follows: (i) the ISAT error tolerance ε_{tol} is 2×10^{-5}, (ii) the number of cells in the domain is 96×96, (iii) the nominal number of particles per cell is 100, and (iv) time averaging is performed over

Table 5
Ranges in z of bins used to evaluate conditional means

Nominal axial location z/D	1	2	3	7.5	15	30	45	60	75
z_{low}/D	0.50	1.51	2.55	7.48	14.7	29.8	44.5	59.8	74.9
z_{up}/D	1.01	2.03	3.07	8.05	15.4	30.6	45.5	60.9	76.2

Table 6
Lower (ξ_l) and upper (ξ_u) limits of the mixture-fraction range, and reference values used in the definition of BI based on different quantities

	H_2O	CO_2	CO	OH	H_2	T
ξ_l	0.35	0.30	0.43	0.28	0.48	0.30
ξ_u	0.45	0.40	0.53	0.36	0.58	0.40
$Y_{\|\xi}$ (or $T_{\|\xi}$)	0.1278	0.1127	0.05745	4.527×10^{-3}	3.639×10^{-3}	2023

at least 2000 time steps after the calculations reach a statistically stationary state (using a moving time average [33]). Extensive numerical tests were performed of flame F using the skeletal mechanism and with C_ϕ modified to $C_\phi = 2.0$ in order to examine the numerical errors in a calculated flame not too close to global extinction. These test cases were performed on grids with 32×32, 48×48, 72×72, and 96×96 cells; with 50, 75, and 100 particles per cell; and with time averaging over at least 2000 steps. The results of these tests show that, with the values of the numerical parameters stated above, the numerical errors are generally no greater than 2% (with respect to the peak value) for the conditional mean temperature and major species, and 5% for the conditional mean minor species, at all investigated locations. It is reasonable to suppose that this level of error—2% for major species and temperature, 5% for minor species—is representative of the numerical errors in the calculations of flames that are not close to global extinction (i.e., flames D and E, and flame F with some mechanisms and larger value of C_ϕ). But for flames close to global extinction (e.g., flame F using the skeletal mechanism and $C_\phi = 1.5$), larger errors are likely, as has already been observed in Fig. 1.

Results are reported below of various means conditional on mixture fraction. At a given nominal axial location, z, these conditional means are formed from all particles in a rectangle in z–r space, extending from $z = z_{low}$ to $z = z_{up}$ and from $r = 0$ to $r = 20D$. The values of z_{low} and z_{up} for the nine output locations are given in Table 5. The conditional means and rms's are then formed in 50 equal-sized bins in mixture-fraction space. At downstream locations ($z/D \geqslant 30$) there are significant statistical fluctuations in some conditional rms's due to the relatively small sample size in some bins (see, e.g., Fig. 12).

Another quantity reported below is the burning index (BI). Following the previous work of Xu and Pope [8], BI is defined as the ratio of the conditional mean (conditioned on mixture fraction being in the range $\xi_l < \xi < \xi_u$) to a reference value obtained using a laminar flame calculation with strain rate 100 s^{-1}. The lower (ξ_l) and upper (ξ_u) limits of the mixture fraction range, and the reference values ($Y_{|\xi}$ and $T_{|\xi}$) used in the definition for BI are listed in Table 6. Burning index is a parameter used to quantify the level of local extinction. Generally speaking, smaller values of BI indicate more local extinction, and BI is essentially zero for a globally extinguished flame.

5. Comparison with previous calculations

It is appropriate to compare the current results with those obtained by Xu and Pope [8] and Tang et al. [9], since the same models are used. First we note the following differences between the three sets of calculations.

- Here the mechanisms used include ARM1 and AMR2, whereas only ARM1 is used in [8] and only ARM2 is used in [9].
- In all calculations, the pilot temperature is set to $T_p = 1880$ K, except that for flame F Xu and Pope use the measured value $T_p = 1860$ K, and here we consider both values, $T_p = 1860$ K and $T_p = 1880$ K (for flame F).
- Radiation is neglected in [8], while here and in [9] calculations are performed both with and without radiation.
- Here the ISAT error tolerance is 2×10^{-5} whereas in [8,9] the value 5×10^{-5} is used (and, in addition, an earlier version of ISAT is used in [8,9]).
- In all three studies, the models and model constants used are identical, with one exception. Here, following [31–34], we use the value $C_{\omega 1} =$

0.65 for this constant in the turbulence frequency model, whereas in [8,9], the value $C_{\omega 1} = 0.56$ is used. This difference is discussed below.

- Updated inlet profiles of mean velocity and Reynolds stresses [44], which are different from those used in [8,9], have been used for the current calculations. The effect of this difference has been tested and found to have a negligible effect on the conditional means.
- A stand-alone particle method implemented in the code PDF2DV was used for previous calculations [8,9]; the hybrid finite-volume/particle method implemented in the code HYB2D [33] is used for the current work. The hybrid algorithm and HYB2D were developed to reduce the bias error observed in PDF2DV, and indeed comparative tests show that (for the same grid size, number of particles, etc.) HYB2D is substantially more accurate [32].
- A different solution domain and a different number of grid cells have been used in the current and previous calculations. A computational domain of $20D \times 80D$ with 96×96 cells is used here, in contrast to the computational domain of $12.5D \times 60D$ with 60×60 cells used in the previous calculations [8,9]. Grid refinements have been performed separately to make sure that both sets of calculations are numerically accurate.
- In the present calculations, time averaging has been performed for a longer time than in the previous calculations.

The different values of $C_{\omega 1}$ used in the different calculations require further comment. This model constant (analogous to $C_{\varepsilon 1}$ in the k–ε model) sensitively controls the calculated spreading rates of jets. In all three sets of calculations the spreading rate is calculated accurately, as evidenced by the accurate mean velocity and mixture-fraction profiles. On the other hand, in the current calculations, if $C_{\omega 1}$ is decreased to 0.56, then markedly inaccurate mean profiles result. Even though both here and in [8] great care is taken to quantify and control the numerical errors, it is difficult to explain these inconsistencies without invoking numerical error. Given the numerical parameters used here compared to [8,9], and given the results of comparative tests of the two codes [32], there are good reasons to suppose that the current calculations based on HYB2D are more accurate.

This issue notwithstanding, it is reassuring to find that in general there is a reasonably good level of agreement between the present and the previous calculations. For example, in Fig. 2 we compare the burning indices obtained in the current and previous calculations of flames D, E, and F. All of these calculations use either the ARM1 or the ARM2 mechanism

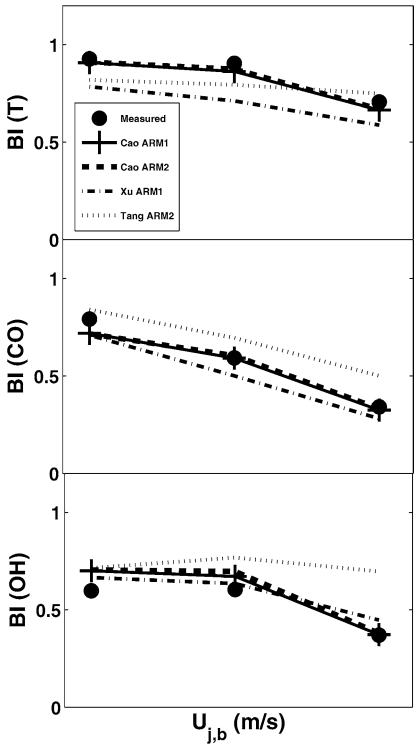

Fig. 2. Burning indices versus jet velocity at $z/D = 15$ for flames D, E, and F. Solid circles, measurements [1,22]. Solid line with plus, the current ARM1 calculations; dashed line, the current ARM2 calculations; dash-dotted line, the previous ARM1 calculations (Xu and Pope [8]); dotted line, the previous ARM2 calculations (Tang et al. [9]). All calculations using EMST with $C_\phi = 1.5$; radiation is omitted; the pilot temperature is set to 1880 K except the flame F calculation of Xu and Pope, in which it is set to 1860 K.

and the EMST mixing model with $C_\phi = 1.5$. The pilot temperature T_p is set to 1880 K except for the flame F calculation of [8], where T_p is set to 1860 K: the effect of radiation is neglected in all calculations. The following observations concerning the current and previous calculations [8,9] are made based on the results shown in Fig. 2.

It is clear that the current calculations using ARM1 and ARM2 are very close to each other, in both major species and minor species. Due to the use of the hybrid method and longer time averaging, the statistical error is less than 2% in these calculations. And these calculations are in excellent agreement with the experimental data.

The calculations in [8,9] differ from each other only in the mechanisms used (ARM1 and ARM2) and in the pilot temperature for flame F (1860 and 1880 K, respectively). Since the only differences between ARM1 and ARM2 is that the latter includes NO chemistry, Tang et al. [9] were surprised by the large

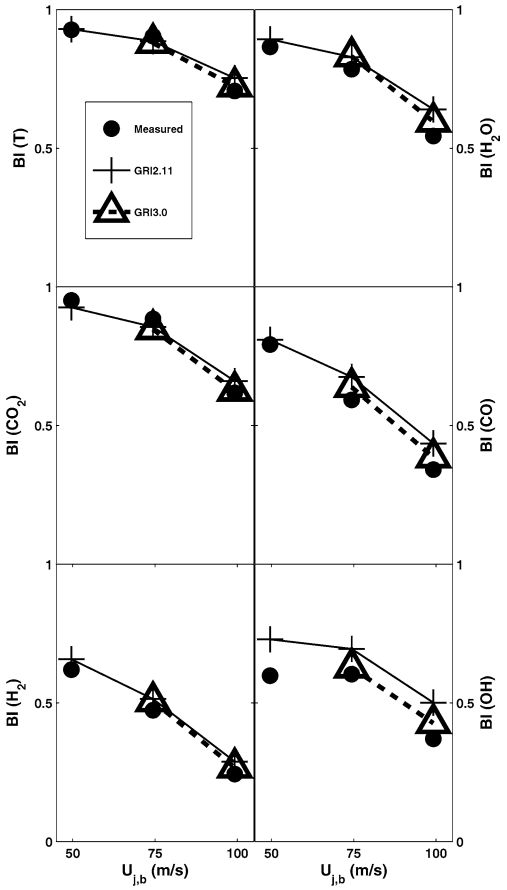

Fig. 3. Burning indices versus jet velocity at $z/D = 15$ obtained using EMST with $C_\phi = 1.5$, and including radiation, for flames D, E, and F. Solid circles, measurements [1,22]. Solid line with plus, GRI2.11; dashed line with triangles, GRI3.0 (flames E and F only). The pilot temperature is set to 1880 K for flames D and E while it is set to 1860 K for flame F.

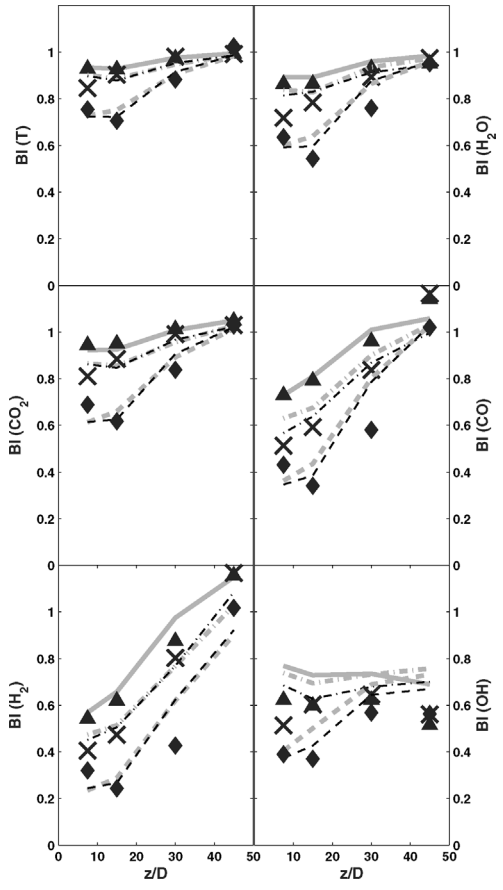

Fig. 4. Burning indices of flames D, E, and F. Symbols, measurements [1,22] for different flames; lines are PDF calculations for different flames. Triangle and solid line, flame D; cross and dash-dotted line, flame E; diamond and dashed line, flame F. The gray lines are obtained using the GRI2.11 mechanism while the black lines for flames E and F are obtained using the GRI3.0 mechanism (GRI3.0 calculations are not reported for flame D). EMST with $C_\phi = 1.5$ is used and radiation is included in these calculations. The pilot temperature is set to 1880 K for flames D and E calculations while it is set to 1860 K for flame F calculations.

difference observed for major species. For flame F, at least part of the observed differences between [8] and [9] can be attributed to the different pilot temperatures used. For flames D and E it is plausible that the difference is due to statistical error which in these calculations is estimated to be about 10% at this location [8,9].

Given the level of statistical error in the previous calculations, and given the sensitivity of flame F to numerical errors, we regard the level of agreement as satisfactory between the current and the previous calculations. Furthermore, none of the conclusions drawn (in Section 7) from the present calculations are in conflict with those drawn in [8,9].

The value of the mixing model constant $C_\phi = 1.5$ was determined by Xu and Pope [8] as that which yields the measured level of local extinction. Since the current calculations are numerically more accurate, and the GRI mechanisms can be supposed to be more accurate than the reduced mechanisms used in [8,9], we verify here that indeed $C_\phi = 1.5$ is the appropriate value.

Figs. 3 and 4 show the calculations of flames D, E, and F using the GRI2.11 and GRI3.0 mechanisms. Radiation is taken into consideration and the pilot temperature T_p is set to the measured values ($T_\mathrm{p} = 1880$ K for the flames D and E, $T_\mathrm{p} = 1860$ K for flame F). The EMST mixing model with $C_\phi = 1.5$ is used for all of these calculations.

As may be seen, for GRI3.0 there is excellent agreement with the experimental data. For GRI2.11

the agreement is in general good, although some differences are evident for BI based on CO and OH. We take these results as verification that $C_\phi = 1.5$ is the appropriate value for the EMST mixing model constant.

Based on the discussion above, unless otherwise stated, the parameters used for the subsequent calculations are set as follows: the EMST mixing model is used with constant $C_\phi = 1.5$; radiation is included; the pilot temperature is set to the experimental values, i.e., 1880 K for flames D and E, and 1860 K for flame F. We refer to this as the "base configuration."

6. Results and discussion

More than 100 joint PDF calculations have been performed for flames D, E, and F using the seven detailed methane mechanisms listed in Table 3. The effects of radiation, pilot temperature, mixing model constant, and reaction rates are investigated by a series of test cases in which these parameters are varied. The calculated unconditional and conditional quantities have been extensively compared with the experimental data. However, due to space limitations, the results shown in this section focus on conditional means in flame F, which has the most significant local extinction and hence it is the most difficult to calculate. For all three flames, we also examine the burning index, which reveals the level of local extinction and successfully characterizes the overall performance of different mechanisms and the sensitivity to different parameters. The key information of 10 or more test cases can be summarized in one plot using burning indices at $z/D = 15$, where the greatest local extinction is observed.

In Section 6.1, plots of burning indices at $z/D = 15$ versus jet velocity are used to investigate the effect of radiation and the pilot temperature. Then in Section 6.2, the performance of all seven mechanisms are investigated. In Section 6.3, concentrating on flame F, the measured and computed unconditional and conditional quantities are shown, and we investigate the sensitivity of these calculations to the changes to the mixing model constant and to the reaction rates. The calculations of NO are shown in Section 6.4. Finally, the joint PDF calculations are related with the autoignition and OPPDIF calculations in Sections 6.5 and 6.6.

6.1. Effect of radiation and pilot temperature

It has been shown in previous studies [9,40] that radiation and the pilot temperature T_p can significantly affect the calculations of flame F. For example, for the calculations with ARM2 in [9], using a pilot temperature of $T_\mathrm{p} = 1880$ K yielded a burning solution; while decreasing the pilot temperature by 20 K (to $T_\mathrm{p} = 1860$ K) resulted in an essentially extinguished solution.

In the current work, to understand better the effect of radiation and the pilot temperature, a systematical study has been performed using the GRI3.0, GRI2.11, ARM1, and ARM2 mechanisms for flames D, E, and F. The results are summarized in Figs. 5 and 6 which show the burning indices (based on T and H_2) versus jet velocity at $z/D = 15$ for these four mechanisms. A burning index equal to zero indicates that the calculation yields a globally extinguished solution.

With the exception of GRI3.0 for flame D, for each of the tested mechanisms and for each flame, three different calculations are shown: first, adiabatic calculations (i.e., with radiation omitted) with $T_\mathrm{p} = 1880$ K; second, radiative calculations with $T_\mathrm{p} = 1880$ K; third, radiative calculations with $T_\mathrm{p} = 1860$ K.

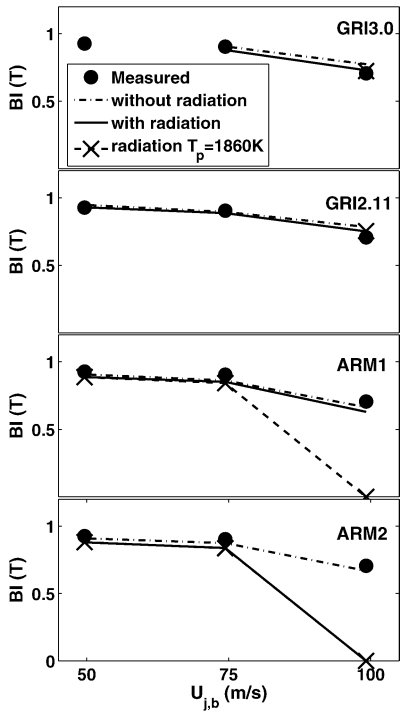

Fig. 5. Burning indices of temperature versus jet velocity at $z/D = 15$. Circles, measurements [1,22]. Lines in the successive plots are PDF calculations using the GRI3.0, GRI2.11, ARM1, and ARM2 mechanisms. Dash-dotted line, calculations without radiation and $T_\mathrm{p} = 1880$ K; solid line, calculations with radiation and $T_\mathrm{p} = 1880$ K; dashed line and cross, calculations with radiation and $T_\mathrm{p} = 1860$ K (mostly indistinguishable from the solid line).

For flames D and E, it is clear from Figs. 5 and 6 that the difference between the three calculations is relatively small: compared to the calculations without radiation, including radiation results in a decrease of at most 4 and 10% in the BI of T and H_2, respectively; while for calculations with radiation, decreasing the pilot temperature by 20 K results in a decrease of at most 2 and 5% in these BIs.

Turning now to flame F, it may be seen that for the calculations with the GRI3.0, GRI2.11, and ARM1 mechanisms, including radiation decreases the burning index of T and H_2 by at most 5 and 17% compared to the adiabatic solution. These changes are somewhat larger than those observed in the calculations of flames D and E.

With GRI3.0 and GRI2.11, decreasing the pilot temperature by 20 K has no discernible effect, whereas it causes the ARM1 calculation to extinguish. This reconfirms the fact that, in these calculations, flame F is very close to global extinction, so it can display extreme sensitivities, and a relatively small change in a physical or numerical parameter can lead to extinction.

For the calculations with ARM2, the heat loss from radiation (with $T_p = 1880$ K) is sufficient to cause global extinction. Compared to ARM1, ARM2 contains additional species related to NO chemistry, and these species depress the temperature slightly—apparently enough to cause extinction.

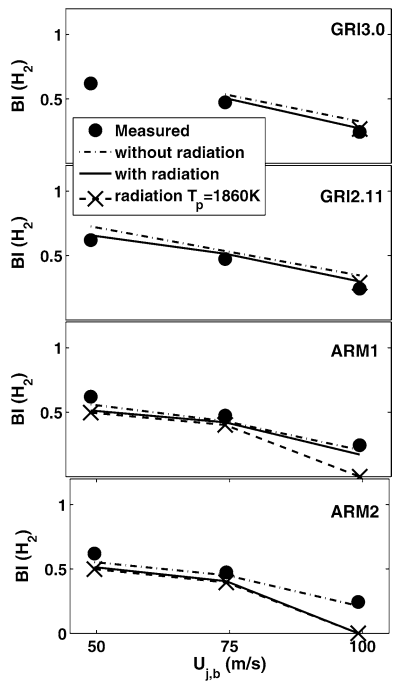

Fig. 6. Burning indices of H_2 versus jet velocity at $z/D = 15$. Symbols and lines, same as Fig. 5.

6.2. Comparison of different mechanisms

The measured and calculated burning indices based on temperature and CO at $z/D = 15$ are plotted against the jet velocity in Figs. 7 and 8 for all seven mechanisms. The base case parameters are used for these calculations, i.e., EMST with $C_\phi = 1.5$, radiation is included, and the value of pilot temperature is set to 1880 K for flames D and E and to 1860 K for flame F.

One can see from Figs. 3 and 4 that burning indices obtained from T, CO_2, and H_2O have similar behavior, and the burning indices obtained from CO, H_2, and OH have similar behavior. So, the burning indices based on T and CO, shown in Figs. 7 and 8, are characteristic of these major and minor species, respectively.

It is clear from Fig. 7 that the S5G211 calculations yield significantly larger values of burning index than the measurements, indicating too little local extinction. On the other hand, the Smooke calculations yield significantly smaller values of burning index than the measurements, corresponding to too much local extinction.

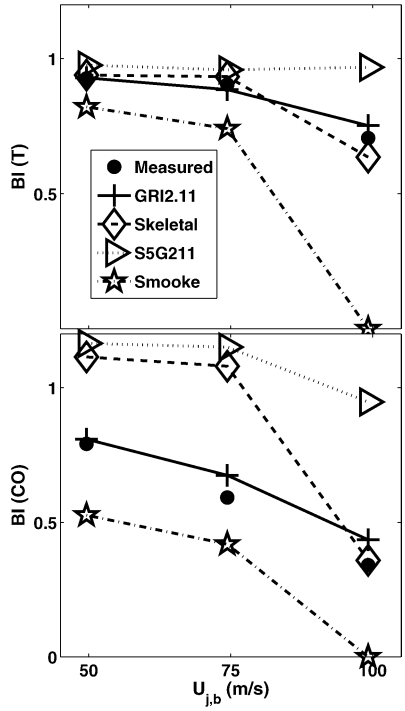

Fig. 7. Burning indices versus jet velocity at $z/D = 15$. Solid circles, measurements [1,22]. Lines with open symbols are PDF calculations. Solid line with plus, GRI2.11; dashed line with diamond, skeletal; dotted line with right triangle, S5G211; dash-dotted line with star, Smooke. $C_\phi = 1.5$, with radiation, $T_p = 1880$ K for flames D and E and $T_p = 1860$ K for flame F.

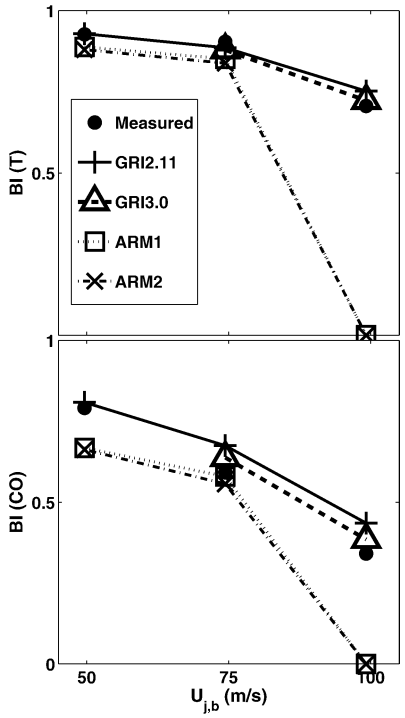

Fig. 8. Burning indices versus jet velocity at $z/D = 15$. Solid circles, measurements [1,22]. Lines with open symbols are PDF calculations. Solid line with plus, GRI2.11; dashed line with triangle, GRI3.0; dotted line with square, ARM1; dash-dotted line with cross, ARM2. $C_\phi = 1.5$, with radiation, $T_\mathrm{p} = 1880$ K for flames D and E and $T_\mathrm{p} = 1860$ K for flame F.

It is also clear from Fig. 7 that in flames D and E the skeletal calculations overpredict the burning index of CO by almost a factor of 2. This is also true for the burning indices of H_2 and OH which are shown in the Supplementary material. Nevertheless, compared to the experimental data, the skeletal mechanism yields quite accurate calculations of BI based on temperature and CO for flame F.

It may be seen from Fig. 8 that both GRI mechanisms yield burning indices for T and CO in good agreement with the experimental data, with GRI3.0 being marginally superior. The two ARM mechanisms yields results almost indistinguishable from each other. As already observed, for flame F (with radiation and $T_\mathrm{p} = 1860$ K) they both lead to global extinction. For flames D and E they generally show good agreement with the experimental data, but the BI for CO in flame D is 17% below the data.

The performance of all seven mechanisms has also been investigated for adiabatic calculations of flames D, E, and F (i.e., with the neglect of radiation). It is found that the omission of radiation changes the agreement with the experimental data slightly, but the relative performance of different mechanisms is essentially the same, no matter whether radiation is included or not.

In summary, the two GRI mechanisms yield comparably good agreement with the experimental data. For flames D and E the ARM mechanisms are somewhat less accurate and they yield extinction for flame F. The remaining mechanisms yield substantial errors (up to 100%) compared to the experimental data, with S5G211 and Smooke consistently underpredicting and overpredicting, respectively, the amount of local extinction. The large errors for the skeletal mechanism in flames D and E suggest that its accurate calculations of BI in flame F are fortuitous.

6.3. *Calculations of flame F*

In this section we focus on flame F which has the highest jet velocity, and hence the strongest turbulence–chemistry interactions. The information contained in the comparison of calculations and measurements of flame F is very useful to test the ability of different turbulent combustion models to represent these complex turbulence–chemistry interactions.

6.3.1. *Sensitivity of flame F*

Because flame F is close to global extinction, calculations of it can display extreme sensitivities to numerical and model parameters, and to uncertainties in the boundary conditions (primarily T_p). The sensitivity to numerical parameters is exemplified by the sensitivity to the ISAT error tolerance which, as shown in Fig. 1, is much stronger in flame F than in flame E. The results in Fig. 5 show that different radiation models (i.e., adiabatic or optically thin) cause calculations with ARM1 to be burning or extinguished, and similarly different pilot temperatures (1880 and 1860 K) yield burning or extinguished solutions with ARM2. Useful conclusions can be drawn from the comparison of measurements and calculations of flame F only if these sensitivities are appropriately accounted for.

Referring again to Fig. 5, we have observed that a small decrease in the pilot temperature or the inclusion of radiation can cause an abrupt transition from a burning solution to an extinguished solution. But note also that the burning solutions exhibit very little sensitivity to the pilot temperature and to the treatment of radiation. And this conclusion is confirmed by the results (Figs. 9–11) later in this section. Hence, despite the uncertainties in the pilot temperature and the treatment of radiation, conclusions can be drawn about those models which yield a burning solution. This is done in the next two subsections, based on unconditional and conditional means, respectively.

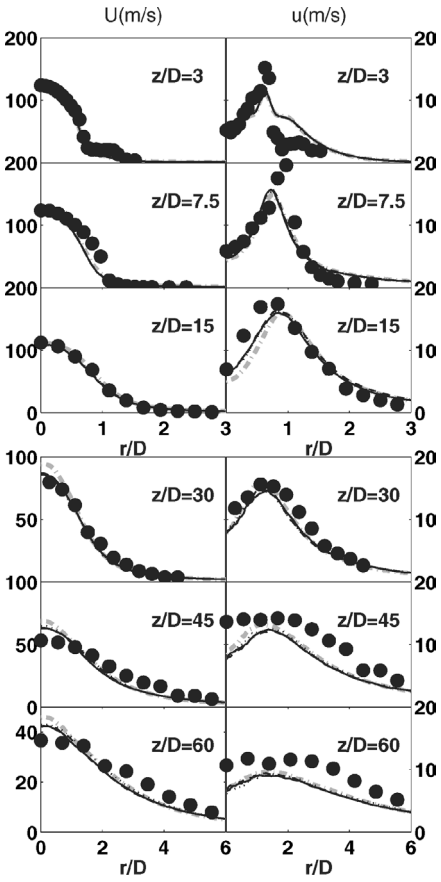

Fig. 9. Computed and measured radial profiles of mean and rms axial velocity in flame F. Circles, measurements [44]; lines, PDF calculations using the EMST mixing model with $C_\phi = 1.5$. Solid line, GRI3.0 calculations with radiation and $T_\mathrm{p} = 1860$ K; dashed line, GRI3.0 calculations with radiation and $T_\mathrm{p} = 1880$ K; dotted line, GRI3.0 calculations without radiation and $T_\mathrm{p} = 1880$ K; gray dash-dotted line, S5G211 calculations with radiation and $T_\mathrm{p} = 1860$ K. (Most lines are indistinguishable at most locations.)

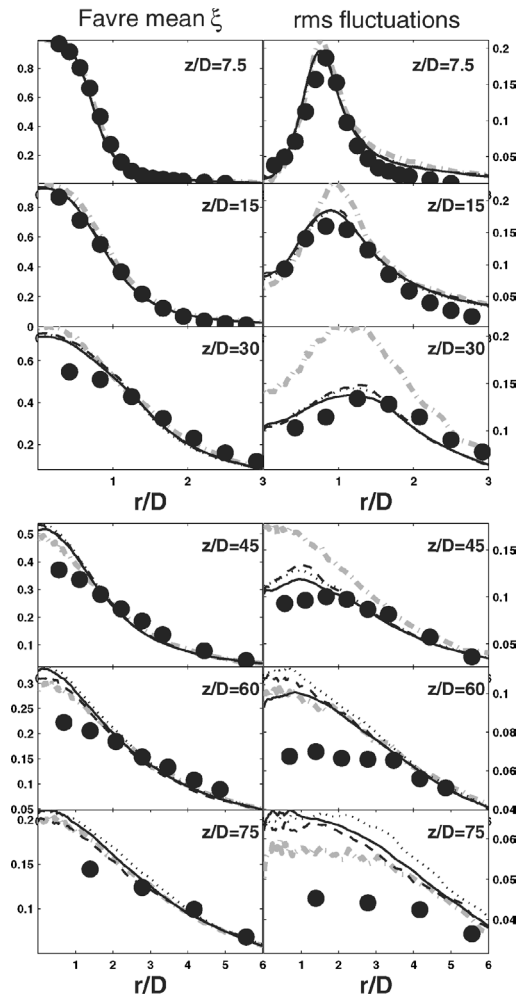

Fig. 10. Computed and measured radial profiles of mean and rms mixture fraction in flame F. The symbols and lines are the same as in Fig. 9.

Because of the strong sensitivity to model parameters, it could be that a particular model produces inaccurate calculations of flame F, and yet a small perturbation to the same model could yield accurate solutions. Perturbations to the reaction rates and to the mixing model constant are examined in Sections 6.3.3 and 6.3.4, respectively, and by doing so it is possible to draw firm conclusions about the inaccuracy of some models.

Figs. 9–11 show radial profiles (at different axial locations) of the unconditional Favre mean and rms velocity, mixture fraction, and temperature. Compared to the experimental data, the calculations shown are of the base configuration using the GRI3.0 and S5G211 mechanism, and also GRI3.0 calculations with T_p increased by 20 K, both with and without radiation.

The correct representation of the velocity and mixture-fraction fields is essential in the calculation of nonpremixed turbulent combustion. Radial profiles of the Favre mean and rms axial velocities are shown in Fig. 9. As may be seen, the three different GRI3.0 calculations are indistinguishable, and are negligibly different from the S5G211 calculations. In general, the agreement among all of the calculations and the experimental data is quite good. The largest differences are for the rms downstream ($z/D = 60$) where the calculated rms is typically 40% lower than the measurements.

Fig. 10 shows the radial profiles of the mean and rms mixture fraction obtained from the four calculations noted above. For the mean there are small

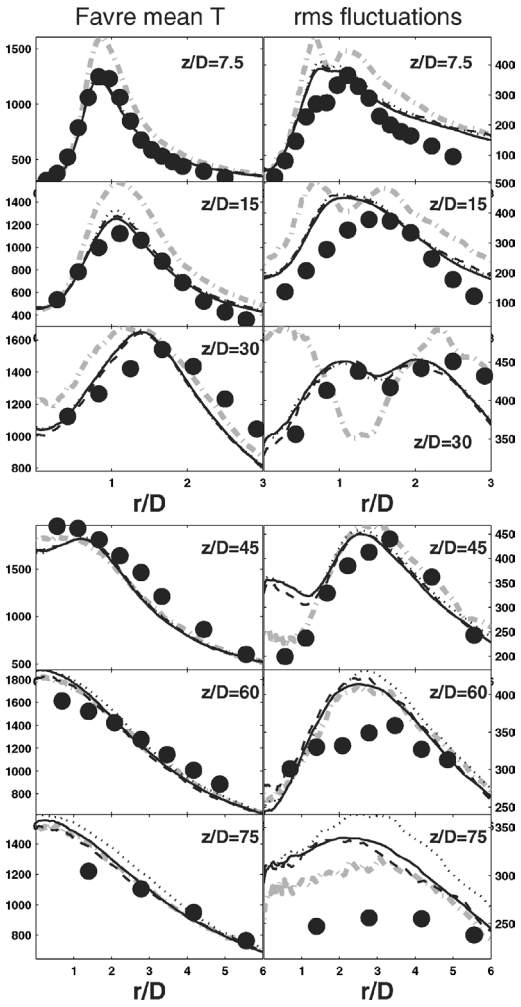

Fig. 11. Computed and measured radial profiles of mean and rms temperature in flame F. The symbols and lines are the same as in Fig. 9.

but discernible differences between the calculations. Downstream ($z/D = 30$) and close to the centerline, the calculations are typically 30% greater than the measurements; but otherwise there is good agreement. For the rms, there are again negligible differences among the three GRI3.0 calculations which agree well with experimental data up to $z/D = 45$, but thereafter yield twice the measured values. In contrast, large inaccuracies in the S5G211 calculations are evident at $z/D = 15$ and $z/D = 30$, where there is most local extinction.

Fig. 11 shows the unconditional Favre mean and rms temperature obtained from the same four calculations as shown in Figs. 9 and 10. There is again little difference among the three GRI3.0 calculations which generally show good agreement with the experimental data up to $z/D = 45$; but there are discrepancies further downstream, especially for the rms. For both the mean and the rms, the S5G211 calculations exhibit significant discrepancies compared to the experimental data in the region of strong turbulence–chemistry interactions ($7.5 \leqslant z/D \leqslant 30$).

In summary, the results shown in Figs. 9–11 confirm that the burning GRI3.0 calculations of flame F are *insensitive* to the pilot temperature and the treatment of radiation; and that, up to $z/D = 45$, the GRI3.0 calculations are accurate compared to the experimental data, whereas the S5G211 calculations are significantly inaccurate.

In the reminder of the paper we focus on means and rms's conditional on mixture fraction. These quantities are more revealing of the turbulence–chemistry interactions and of the differences between the mechanisms.

6.3.2. *Calculation of conditional quantities*

With the use of base case configuration (i.e., $T_\mathrm{p} = 1860$ K, the inclusion of radiation, and $C_\phi = 1.5$), the GRI3.0, GRI2.11, skeletal, and S5G211 mechanisms yield burning solutions for flame F. For these mechanisms, the conditional mean temperature and the conditional mean mass fractions of CO and OH are examined in this subsection. On the other hand, the ARM2, the ARM1, and the Smooke mechanisms yield globally extinguished solutions for flame F with the base case configuration, and so are not considered here.

Fig. 12 shows the measured and computed conditional mean and rms temperature obtained using the four mechanisms yielding burning solutions. The results obtained with the GRI3.0, GRI2.11, and skeletal mechanisms are very similar to each other and are generally in good agreement with the experimental data, although the conditional rms is underpredicted for rich mixtures ($\xi > 0.5$) at $z/D = 7.5$ and 15. On the other hand, S5G211 substantially overpredicts the conditional mean temperature—by up to 550 K—and underpredicts the rms.

Similar observations apply to the conditional means and rms's of the mass fractions of CO and OH which are shown in Figs. 13 and 14. Here, however, some differences are evident between the skeletal and the GRI mechanisms (e.g., the rms of CO at $z/D = 30$ and the mean of OH at $z/D = 45$), with the results of the skeletal mechanism showing greater deviations from the experimental data.

In summary, for the results shown in Figs. 12–14, the GRI3.0 and GRI2.11 calculations are generally similar to each other and are in reasonably good agreement with the experimental data. This is true for other species (except NO), and also for the calculations of flames D and E (which are shown in the Supplementary material). On the other hand, while

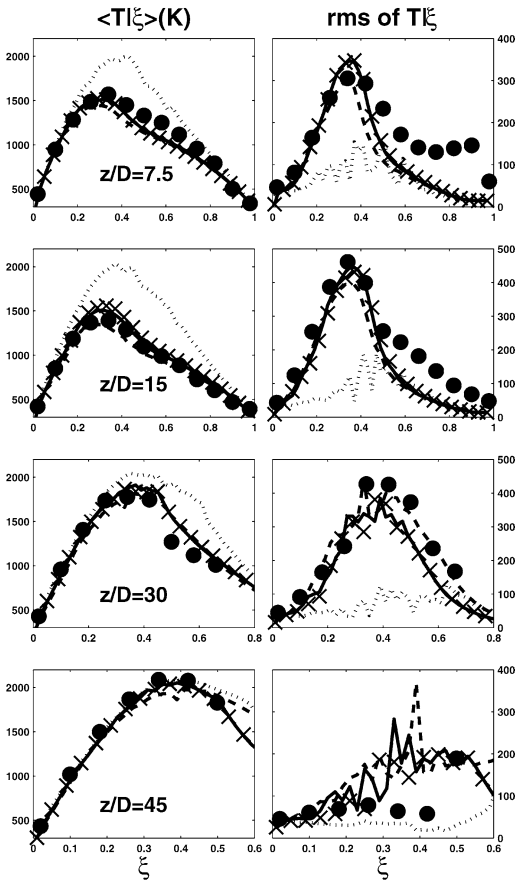

Fig. 12. Measured and computed conditional mean and rms temperature obtained in the flame F calculations ($C_\phi = 1.5$, $T_\mathrm{p} = 1860$ K, with radiation) using different mechanisms. Measurements [22] are shown by solid circles and mechanisms used are: GRI3.0 (solid line), GRI2.11 (cross), skeletal (dashed line), and S5G211 (dotted line).

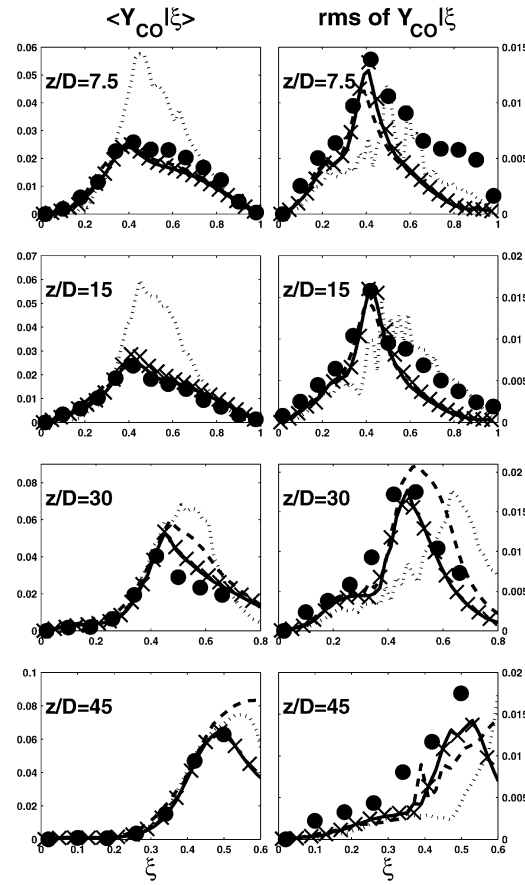

Fig. 13. Measured and computed conditional mean and rms mass fraction of CO in flame F using different mechanisms. The symbols and lines are the same as in Fig. 12.

the skeletal mechanism yields generally reasonable calculations of the conditional means of CO and OH, these quantities are typically overpredicted by a factor of 2 in flames D and E (see Fig. 7 and the Supplementary material).

6.3.3. Sensitivity to reaction rates

We have seen that the GRI3.0, GRI2.11, and skeletal mechanisms yield reasonably accurate calculations of flame F in the base configuration, and that ARM1 and ARM2 do so with perturbed pilot temperature or radiation treatment. But S5G211 yields inaccurate calculations, while with the Smooke mechanism extinguished solutions are obtained for all pilot temperatures and radiation treatments considered. As discussed in Section 6.1, for mechanisms that yield inaccurate solutions (i.e., S5G211 and Smooke) it is important to determine if a slightly perturbed model can yield accurate solutions.

To this end, in Fig. 15 we show results obtained with the S5G211 and Smooke mechanisms with substantial perturbations. Specifically, all reaction rates in the S5G211 mechanism are decreased by a factor of 10, while those in the Smooke mechanism are doubled and tripled. (In practice, changing all rates by a factor α is achieved by changing the time step Δt in the reaction fractional time step to $\alpha \Delta t$.)

It may be seen from Fig. 15 that the standard S5G211 mechanism substantially overpredicts the conditional mean temperature at $z/D = 15$, in fact, by up to 550 K. Reducing the reaction rates by a factor of 10 reduces the conditional mean temperature (as expected); but it is still overpredicted by up to 350 K.

For the Smooke mechanism, burning solutions are obtained by doubling and tripling the reaction rates. But with them doubled, the conditional mean temperature is overpredicted by up to 350 K at $z/D = 15$. It is natural to seek a smaller perturbation that yields a burning solution with a lower conditional mean temperature—in better agreement with the ex-

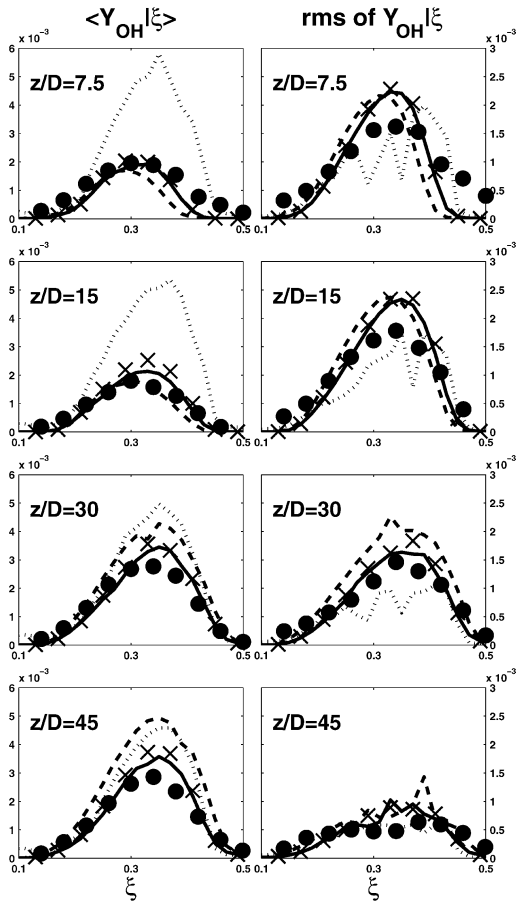

Fig. 14. Measured and computed conditional mean and rms mass fraction of OH in flame F using different mechanisms. The symbols and lines are the same as in Fig. 12.

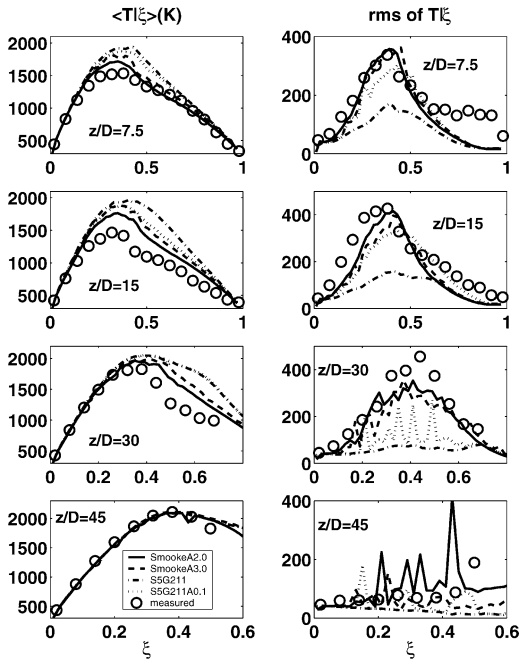

Fig. 15. The effect of reactions rates investigated using the measured and computed conditional mean and rms temperature in flame F. Circles, measurements [1,22]; lines, joint PDF calculations (adiabatic, $C_\phi = 1.5$, $T_\mathrm{p} = 1880$ K) using the Smooke mechanism with doubled reaction rates (solid), tripled reaction rates (dashed), and the S5G211 mechanism with the standard reaction rates (dash-dotted) and tenth reaction rates (dotted).

perimental data. But with the reaction rates increased by a factor of 1.9 we are unable to obtain a burning solution. Note the strong sensitivity to decreasing this factor from 2.0 to 1.9, compared to the modest sensitivity observed in Fig. 15 to increasing the factor from 2 to 3.

It can clearly be concluded, therefore, that accurate calculations of flame F cannot be achieved by a small perturbation to either the S5G211 or the Smooke mechanisms.

6.3.4. Sensitivity to the mixing model constant C_ϕ

With the same motivation as in the previous subsection, we examine here the sensitivity of the calculations using the different mechanisms to the value of the mixing model constant C_ϕ. This is the only model constant directly affecting the compositions.

Fig. 16 shows the conditional mean and rms temperature obtained using the S5G211 mechanism with the values $C_\phi = 1.2$, 1.4, 1.5, and 2.0. Several observations can be made. First, decreasing C_ϕ results in a decrease in the conditional means and an increase in the rms's, as has previously been observed [8,16]. Second, with $C_\phi = 1.2$ the results are generally in good agreement with the experimental data, and are very similar to those obtained with ARM2 (with $C_\phi = 1.5$). Third, the calculations become more sensitive to changes in C_ϕ when they are closer to global extinction. Fourth, compared to the results shown in Fig. 15, starting from the same case (the S5G211 mechanism and EMST with $C_\phi = 1.5$), a 20% change in the value of C_ϕ (from 1.5 to 1.2) yields a much larger difference than decreasing the reaction rates by a factor of 10. This indicates that (for the S5G211 mechanism and the parameters used), the calculations are much more sensitive to the mixing model constant than to the chemical reaction rates. The reason for this is not evident and is deserving of further investigation.

Similar tests have been performed for all other mechanisms. The maxima (over mixture fraction) of the conditional mean and rms temperatures for different values of C_ϕ are shown in Fig. 17. One may see that the change of the maximum temperatures with the change of C_ϕ has a similar trend for all mechanisms. First, decreasing C_ϕ results in decreasing

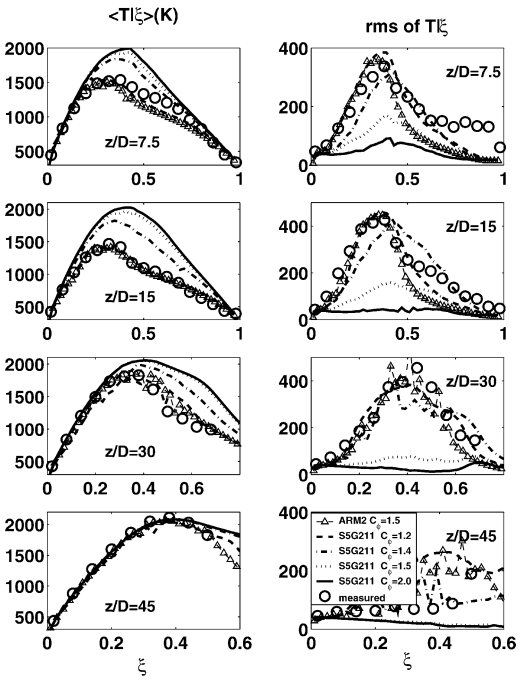

Fig. 16. Effect of the mixing model constant C_ϕ investigated using the measured and computed conditional mean and rms temperatures in flame F using different mechanisms and EMST mixing model with different values of C_ϕ. Circles, measurements [1,22]; lines, joint PDF calculations (adiabatic, $T_p = 1880$ K) using the ARM2 mechanism with $C_\phi = 1.5$ (dashed line with triangle), and the S5G211 mechanism with the value of C_ϕ set to 1.2 (dashed), 1.4 (dash-dotted), 1.5 (dotted), and 2.0 (solid).

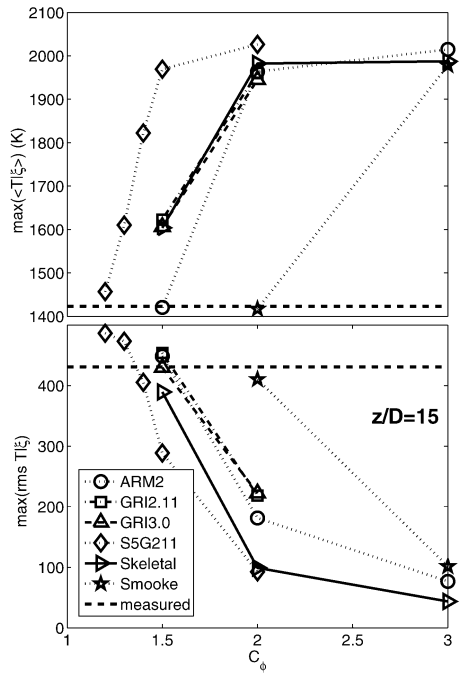

Fig. 17. Sensitivity of joint PDF calculations to the value of C_ϕ in flame F: maximum conditional mean and rms temperature at $z/D = 15$ against C_ϕ. Horizontal dashed lines are the experimental data and lines with symbols represent different mechanisms. All calculations are adiabatic calculations with $T_p = 1880$ K.

the conditional means and increasing the conditional rms's. Second, the calculations are more sensitive to the change of C_ϕ when they are closer to global extinction. Third, for several of the mechanisms (the Smooke, ARM2, and skeletal mechanisms), the value of C_ϕ yielding the measured value of the conditional mean also yields the measured value of the conditional rms.

The finding is, therefore, that, with a perturbation to C_ϕ, accurate calculations of the peak conditional temperature in flame F can be obtained using the S5G211 mechanism ($C_\phi = 1.2$) and with the Smooke mechanism ($C_\phi = 2.0$).

What is to made of this finding? For a given mixing model (here EMST), there should be a single value of C_ϕ: there is no physical basis for supposing that a different value of C_ϕ is appropriate for use with different chemical mechanisms. There are several reasons (see, e.g., [47]) to suppose that the GRI mechanisms—although not perfect—provide an adequate representation of the C–H–O chemistry in these flames; certainly more so than the overly reduced S5G211 mechanism, and the skeletal and Smooke mechanisms which have no representation of C_2 and C_3 species. Hence we take the present results from Fig. 17 for GRI3.0, GRI2.11, ARM1, and ARM2 as reconfirmation that $C_\phi = 1.5$ is the appropriate value for EMST. Using $C_\phi = 1.2$ with S5G211 or $C_\phi = 2.0$ with the Smooke mechanism should therefore be viewed as introducing an error to compensate for deficiencies in these mechanisms.

6.4. Calculations of NO

Accurate calculations of NO are very important for the application of turbulent combustion models to pollutant control. Fig. 18 shows the conditional mean and rms of the mass fraction of NO at different axial locations in flame E for base-configuration calculations using the ARM2, GRI2.11, GRI3.0, and S5G211 mechanisms. (The other three mechanism do not represent NO chemistry.) We use flame E for this aspect of the investigation so that the performance of all four mechanisms which include NO chemistry can be compared: for flame F, ARM2 yields global extinction (for the base case configuration).

One can easily see that the S5G211 mechanism overrepresents the conditional mean mass fraction

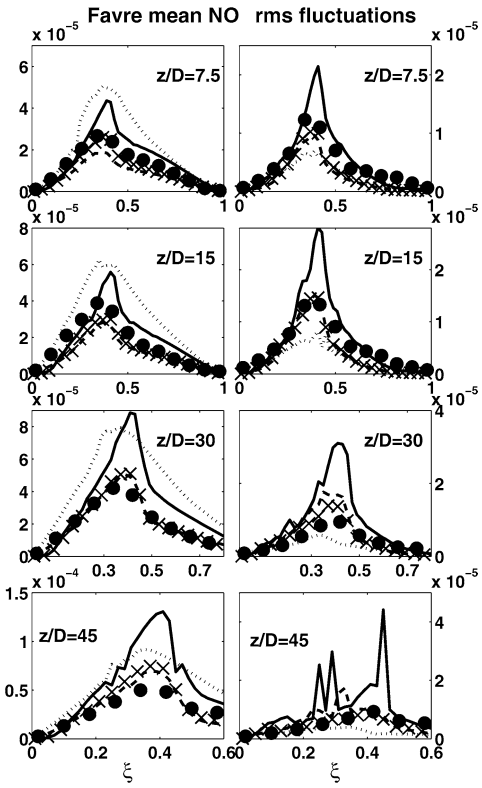

Fig. 18. Measured and computed conditional mean and rms mass fraction of NO obtained in flame E using the base case configuration. Solid circles are measurements [1,22] and others lines and symbols are PDF calculations using different mechanisms: GRI3.0 (solid line), GRI2.11 (cross), ARM2 (dashed line), and S5G211 (dotted line).

of NO, typically by a factor of 2 compared to the measurements. The calculations using GRI3.0 yield significantly higher levels of NO than the measurements—higher by a factor of up to 2.4 at $z/D = 45$. This substantial overprediction of NO is also observed in the current calculations of flames D and F (shown in the Supplementary material), as well as in previous calculations of flame D [17] and of laminar nonpremixed flames [47].

The ARM2 and GRI2.11 calculations are generally very close to each other and have reasonable agreement with the measurements. This is also true for the calculations of flames D and F (except that ARM2 yields global extinction for flame F with the base case configuration). This is consistent with the laminar flame studies performed by Barlow et al. [47] and the composition PDF calculations of flame D performed by Raman et al. [17] and the joint PDF calculations of Tang et al. [9].

While the pilot temperature has a negligible effect on the calculations of NO, including radiation can decrease the peak value of the conditional mean NO

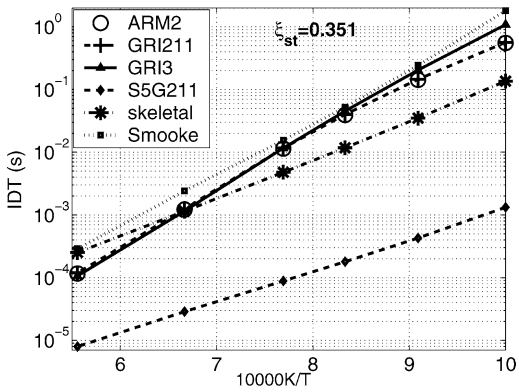

Fig. 19. Ignition delay times (IDTs) of different mechanisms at different initial temperatures, T.

by up to 25%. The relative tendencies obtained from including or neglecting radiation are essentially the same for flames D, E, and F (as may be seen in the Supplementary material).

6.5. *Autoignition test*

In this and the next subsection, we compare the relative performance of the mechanisms in simple test cases, and relate the observed behavior in these tests to that in the calculations of flames D, E, and F.

Autoignition tests have been performed for a mixture of the Barlow and Frank fuel (25% methane, 75% air) and air at the stoichiometric mixture fraction ($\xi_{st} = 0.351$) for all seven mechanisms. The ignition delay times (IDTs) obtained using different initial temperatures are shown in Fig. 19. The IDTs of the ARM1 mechanism are almost identical to those of the ARM2 mechanism and are not shown in the figure. The S5G211 mechanism has much shorter IDTs than the other mechanisms, e.g., 13 to 820 times shorter than those of GRI3.0. On the other hand, the Smooke mechanism has the longest IDTs for all initial temperatures. The IDTs of the ARM2, GRI2.11, and GRI3.0 mechanisms are generally close to each other, although the IDTs for GRI3.0 are somewhat longer at low temperatures. Compared to the GRI mechanisms, the IDTs of the skeletal mechanism are shorter at low temperatures, but longer at high temperatures.

The relative behavior of different mechanisms in the joint PDF calculations (characterized by burning indices, Figs. 7 and 8, and conditional mean temperature, Fig. 12) can be related to their IDTs (shown in Fig. 19). In general, the shorter the IDT, the larger the burning indices, and the higher the conditional mean temperature. This is consistently the case for the S5G211 mechanism (with the shortest IDTs), for

Table 7
Parameters for the laminar opposed-flow nonpremixed flame calculations with nominal strain rate $a \equiv (U_{fu} + U_{ox})/D = 50\ s^{-1}$

	Mole fraction			Temperature	Velocity	Pressure	Distance D
	CH_4	N_2	O_2	(K)	(cm/s)	(atm)	(cm)
Fuel	0.25	0.5925	0.1575	300	50 (U_{fu})	1	2
Oxidizer	0.0	0.79	0.21	300	50 (U_{ox})	1	

the Smooke mechanism (with the largest IDTs), and for the GRI3.0, GRI2.11, ARM1, and ARM2 mechanisms, considered together as a group (which have intermediate IDTs).

The behavior of the skeletal mechanism is more complex and does not conform simply to the pattern observed above for the other mechanisms. Relative to the GRI mechanisms, we observe from Fig. 19 that the skeletal mechanism has a short IDT at low temperatures and a long IDT at high temperatures, while we observe from Fig. 7 that it has higher burning indices for flames D and E, but lower burning indices for flame F. To maintain the consistent pattern, one would have to contend that a low-temperature IDT is relevant to flames D and E, and a high-temperature IDT to flame F; whereas, if anything, the physics of the problem suggests the opposite—given the relatively lower temperatures in flame F.

6.6. *Opposed-flow nonpremixed laminar flame test*

In order to relate the performance of these mechanisms in turbulent combustion to that in laminar combustion, calculations have been performed using the GRI2.11, GRI3.0, skeletal and Smooke mechanisms for a steady, laminar, axisymmetric nonpremixed flame between two opposed jets of equal (but opposite) velocity. The OPPDIF code [24] coupled in the commercial software package CHEMKIN 3.7 is used for these calculations. The configuration and parameters used for these tests are listed in Table 7. The composition of the fuel stream is the same as that in the Barlow and Frank turbulent flames, namely 25% methane and 75% air. While the configuration is, therefore, partially premixed, as previously observed [1,47], the combustion occurs in a nonpremixed mode. The mixture-averaged formula is used for diffusion velocities. (Calculations using the reduced mechanisms ARM1, ARM2, and S5G211 cannot readily be performed using this version of OPPDIF.)

The maxima of the temperature, and of the mass fractions of CO, OH and NO obtained using different values of nominal strain rate are shown in Fig. 20. The right-most points for different mechanisms represent the nominal extinction strain rates, which are 250, 350, 350, and 375 s^{-1} for the Smooke, GRI2.11, GRI3.0, and skeletal mechanisms, respectively: at strain rates of 25 s^{-1} greater than these values the flames are extinguished.

For the Smooke and GRI mechanisms, the pattern observed above is naturally extended: relative to the GRI mechanism, the Smooke mechanism has a longer IDT, a smaller extinction strain rate, and correspondingly lower burning indices and conditional mean temperatures in the turbulent flames.

The relative behaviors of the skeletal and GRI mechanisms are the same in the laminar flames and turbulent flames in the following respects. In the laminar flames, the peak temperatures are comparable (at least for strain rates above 50 s^{-1}), as are the BIs based on temperature (see Fig. 7). On the other hand, the skeletal mechanism yields significantly higher levels of CO and OH both in the laminar flames (Fig. 20) and in the turbulent flames, as revealed by

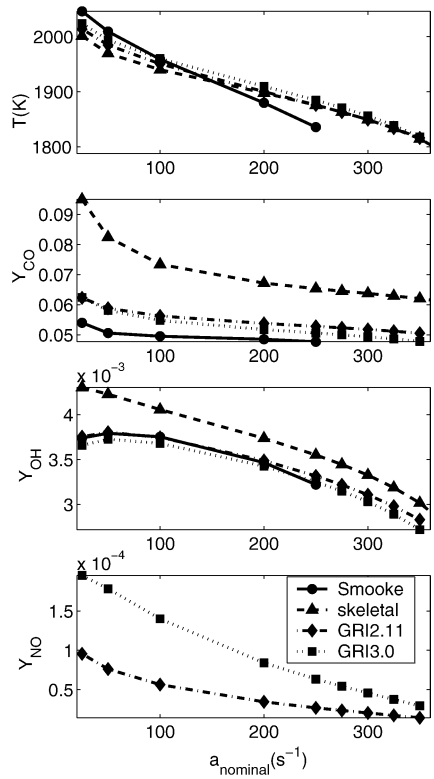

Fig. 20. Peak values of temperature, and mass fractions of CO, OH, and NO against the nominal strain rate a obtained in laminar opposed-flow diffusion flame calculations.

the BIs based on CO shown in Fig. 7 and on OH (shown in the Supplementary material).

It has been shown in previous studies [47] that calculations of laminar opposed-flow partially premixed methane/air flames using GRI3.0, GRI2.11, ARM2, and ARM1 mechanisms yield similar results for major species, while there may be significant differences for minor species. The current calculations are in accord with these results. It is clearly shown in Fig. 20 that the GRI3.0 calculations yield about two times higher levels of NO when compared with the GRI2.11 calculations. This is consistent with the joint PDF calculations shown in Fig. 18.

7. Summary and conclusions

A comprehensive study has been conducted on the performance of seven different chemical mechanisms used in joint PDF model calculations of the Barlow and Frank [1] nonpremixed piloted jet flames D, E, and F. The seven mechanisms (GRI3.0, GRI2.11, ARM2, ARM1, S5G211, skeletal, and Smooke) range from the 53-species GRI3.0 mechanism to a 5 step reduced mechanism (S5G211): details are given in Tables 3 and 4. As in many previous studies [8,9, 31–35], the PDF model is based on the joint PDF of velocity, turbulence frequency, and composition. It uses the simplified Langevin model [29] for velocity; the Jayesh–Pope model [30] for turbulence frequency; and the EMST mixing model [11] for the compositions, all with the standard model constants given in Table 2. The Supplementary material contains many more results of these PDF calculations than can be shown here.

The modeled joint PDF equation is solved using the hybrid finite-volume/particle method implemented in the code HYB2D [31,33,35], and the chemistry is implemented using the ISAT algorithm [45]. The results of numerical tests are reported (varying the grid size, number of particles, ISAT error tolerance, and time-averaging period) to establish the numerical accuracy of the calculations. For flames not close to global extinction, the numerical errors in conditional means of temperature and major species are generally no greater than 2%, and for minor species no greater than 5%. The large number of numerically-accurate PDF calculations reported here demonstrate that this PDF/ISAT methodology can be effectively applied to turbulent flames using chemical mechanisms with of order 50 species.

The performance of the seven different chemical mechanisms is examined through comparison of the PDF model calculations with the experimental data, including unconditional and conditional means and rms's, and the burning index (BI). The principal conclusions are as follows.

(1) For temperature and species (excluding NO), the two GRI mechanisms yield comparably good agreement with the experimental data for all three flames.
(2) For flames D and E, the two ARM mechanisms yield results very similar to each other, with slightly worse agreement with the experimental data compared to GRI. For flame D, for example, the ARM calculations of BI based on CO are 17% below the measurement (at $z/D = 15$).
(3) For flame F (and the base configuration) both ARM mechanisms yield global extinction. However, with the relatively small perturbations of an increasing in 20 K of the pilot temperature and the neglect of radiation, both ARM mechanisms yield burning solutions in good agreement with the experimental data.
(4) The ARM2 mechanism and the GRI2.11 mechanism on which it is based provide reasonably accurate calculations of NO (see Fig. 20). However, consistent with previous observations [17, 47], the GRI3.0 mechanism overpredicts NO, typically by a factor of 2.
(5) The other three mechanism (S5G211, skeletal, and Smooke) display significant inaccuracies. Fig. 7, for example, shows that S5G211 grossly underestimates the level of local extinction; whereas the Smooke mechanism overpredicts local extinction in flames D and E and yields global extinction for flame F. The skeletal mechanism shows fortuitous agreement for flame F, but is quite inaccurate for flames D and E.
(6) Moderate perturbations to the Smooke and S5G211 mechanisms are incapable of yielding agreement with the experimental data. Even if all rates in the S5G211 mechanism are decreased by a factor of 10, local extinction is still grossly overpredicted (see Fig. 15).
(7) The predicted level of local extinction is sensitive to the value specified for the EMST mixing model constant C_ϕ, with this level increasing with decreasing C_ϕ (see Fig. 17). The calculations with the GRI and ARM mechanisms reconfirm that $C_\phi = 1.5$ is the appropriate value, as first determined by Xu and Pope [8] and consistently used thereafter. With $C_\phi = 1.2$ and $C_\phi = 2.0$ the S5G211 and Smooke mechanisms, respectively, yield the correct level of local extinction in flame F. However, these changes to C_ϕ should be regarded as inappropriate additions of compensating errors, to compensate for deficiencies in the mechanisms.

(8) To an extent there is a consistent pattern among the ignition delay times, laminar flame properties, and the turbulent flame calculations for the different mechanisms. Compared to the GRI and ARM mechanisms, the Smooke mechanism has a long IDT, a small extinction strain rate, and it consistently overpredicts local extinction in the turbulent flames. Conversely, S5G211 has, comparatively, a very short IDT, and it grossly underpredicts local extinction. Compared to GRI2.11, in the laminar flames GRI3.0 overpredicts NO (typically by a factor of 2), and the skeletal mechanism significantly overpredicts CO and OH. These same discrepancies are also observed in the conditional means in the turbulent flames.

It should be appreciated that the strength and reliability of the conclusions drawn above depend on studying the mechanisms over the range of flames and for perturbed conditions. A study of flame F alone might conclude that the skeletal mechanism is satisfactory, whereas the results for flames D and E clearly show this not to be the case. Or, if only the base configuration were studied it might be concluded that ARM1 is unsatisfactory in that it yields global extinction for flame F. But as shown in Fig. 5, with a 20 K increase in the pilot temperature—well with the experimental uncertainty of 50 K—the ARM1 mechanism yields a burning solution, in good agreement with the experimental data.

These calculations again demonstrate the value of the piloted jet flames (using the Sydney burner geometry) in the study of turbulence–chemistry interactions. The experiments performed on these flames have been central to the advances made over the last decade in our abilities to model accurately turbulence–chemistry interactions in such flames.

Acknowledgments

This paper is dedicated to Bob Bilger on the occasion of his seventieth birthday. The authors are grateful to Profs. A.R. Masri and D.A. Caughey for valuable discussions and suggestions during the course of the research. This work is supported by Air Force Office of Scientific Research under Grant F-49620-00-1-0171 and the Department of Energy under Grant DE-FG02-90ER. The computations were conducted using the resources of the Cornell Theory Center, which receives funding from Cornell University, New York State, federal agencies, foundations, and corporate partners.

Supplementary material

Supplementary data for this article may be found in the online version at doi: 10.1016/j.combustflame.2005.08.018.

References

[1] R.S. Barlow, J.H. Frank, Proc. Combust. Inst. 27 (1998) 1087–1095.
[2] S.H. Stärner, R.W. Bilger, Combust. Flame 61 (1985) 29–38.
[3] R.W. Bilger, S.B. Pope, K.N.C. Bray, J.F. Driscoll, Proc. Combust. Inst. 30 (2005) 21–42.
[4] A.R. Masri, R.W. Bilger, Proc. Combust. Inst. 21 (1986) 1511–1520.
[5] A.R. Masri, R.W. Dibble, R.S. Barlow, Prog. Energy Combust. Sci. 22 (1996) 307–362.
[6] A.N. Karpetis, R.S. Barlow, Proc. Combust. Inst. 29 (2002) 1929–1936.
[7] R.S. Barlow, private communication (2005).
[8] J. Xu, S.B. Pope, Combust. Flame 123 (2000) 281–307.
[9] Q. Tang, J. Xu, S.B. Pope, Proc. Combust. Inst. 28 (2000) 133–139.
[10] R.P. Lindstedt, S.A. Louloudi, E.M. Váos, Proc. Combust. Inst. 28 (2000) 149–156.
[11] S. Subramaniam, S.B. Pope, Combust. Flame 115 (1998) 487–514.
[12] R.L. Curl, AIChE J. 9 (1963) 175–181.
[13] J. Janicka, W. Kolbe, W. Kollmann, J. Non-Equilib. Thermodyn. 4 (1979) 47–66.
[14] Z. Ren, S.B. Pope, Combust. Flame 136 (2004) 208–216.
[15] S. Mitarai, J.J. Riley, G. Kosály, Phys. Fluids 15 (2003) 3856–3866.
[16] R.P. Lindstedt, S.A. Louloudi, Proc. Combust. Inst. 29 (2002) 2147–2154.
[17] V. Raman, R.O. Fox, A.D. Harvey, Combust. Flame 136 (2004) 327–350.
[18] H. Wang, Y. Chen, Chem. Eng. Sci. 59 (2004) 3477–3490.
[19] H.P. Mallampalli, T.H. Fletcher, J.Y. Chen, Paper 96F-098, presented at the Fall Meeting of the Western States Section of the Combustion Institute, University of Southern California, Los Angeles, CA, October 28–29, 1996.
[20] C.J. Sung, C.K. Law, J.Y. Chen, Proc. Combust. Inst. 27 (1998) 295–304.
[21] GRI-Mech web site, http://www.me.berkeley.edu/gri-mech.
[22] R.S. Barlow (Ed.), Web site for the International Workshop on Measurement and Computation of Turbulent Non-premixed Flames (TNF), Sandia National Laboratories, http://www.ca.sandia.gov/tdf/Workshop.
[23] R.S. Barlow, J.H. Frank, Piloted CH4/Air Flames C, D, E, and F, Release 2.0, 2003, http://www.ca.sandia.gov/tdf/Workshop.
[24] Reaction Design, OPPDIF Application User Manual, Release 3.7.1, 2003.
[25] S.B. Pope, Prog. Energy Combust. Sci. 11 (1985) 119–192.

[26] R. Cao, S.B. Pope, J. Comput. Phys. 185 (2003) 194–212.
[27] J.Y. Chen, W.C. Chang, Combust. Sci. Technol. 133 (1998) 343–375.
[28] A.R. Masri, R. Cao, S.B. Pope, G.M. Goldin, Combust. Theory Modelling 8 (2004) 1–22.
[29] D.C. Haworth, S.B. Pope, Phys. Fluids 29 (1986) 387–405.
[30] P.R. Van Slooten, Jayesh, S.B. Pope, Phys. Fluids 10 (1998) 246–265.
[31] R. Cao, S.B. Pope, A.R. Masri, Combust. Flame 142 (2005) 438–453.
[32] P. Jenny, M. Muradoglu, K. Liu, S.B. Pope, D.A. Caughey, J. Comput. Phys. 169 (2001) 1–23.
[33] M. Muradoglu, S.B. Pope, D.A. Caughey, J. Comput. Phys. 172 (2001) 841–878.
[34] M. Muradoglu, K. Liu, S.B. Pope, Combust. Flame 132 (2003) 115–137.
[35] K. Liu, S.B. Pope, D.A. Caughey, Combust. Flame 141 (2005) 89–117.
[36] S.B. Pope, Turbulent Flows, Cambridge Univ. Press, Cambridge, UK, 2000.
[37] S. James, M.S. Anand, M.K. Razdan, S.B. Pope, J. Eng. Gas Turbines Power Trans. ASME 123 (2001) 747–756.
[38] M.D. Smooke, I.K. Puri, K. Seshadri, Proc. Combust. Inst. 21 (1986) 1783–1792.
[39] B.A.V. Bennett, M.D. Smooke, private communication (2004).
[40] Q. Tang, Ph.D. thesis, Cornell University, 2003.
[41] W.L. Grosshandler, RADCAL: A Narrow-Band Model for Radiation in a Combustion Environment, NIST Technical Note 1402, 1993.
[42] J.H. Frank, R.S. Barlow, C. Lundquist, Proc. Combust. Inst. 28 (2000) 447–454.
[43] R.S. Barlow, N.S.A. Smith, J.Y. Chen, R.W. Bilger, Combust. Flame 117 (1999) 4–31.
[44] Ch. Schneider, A. Dreizler, J. Janicka, E.P. Hassel, Combust. Flame 135 (2003) 185–190.
[45] S.B. Pope, Combust. Theory Modelling 1 (1997) 41–63.
[46] B.J.D. Liu, S.B. Pope, Combust. Theory Modelling (2005), in press.
[47] R.S. Barlow, A.N. Karpetis, J.H. Frank, J.Y. Chen, Combust. Flame 127 (2001) 2102–2118.